Study of the interaction mechanism between hydrophilic thiol capped gold nanoparticles and melamine in aqueous medium

Sara Cerra, [a,*] Tommaso A. Salamone,[a] Fabio Sciubba,[a] Martina Marsotto,[b] Chiara Battocchio,[b] Silvia Nappini,[c] Francesca A. Scaramuzzo,[d] Roberto Li Voti,[d] Concita Sibilia, [d] Roberto Matassa,[e] Ana Maria Beltrán,[f] Giuseppe Familiari,[e] Ilaria Fratoddi[a,*]

[a] Department of Chemistry, Sapienza University of Rome, P.le A. Moro 5, 00185 Rome, Italy

[b] Department of Sciences and CISDiC, Roma Tre University, via della Vasca Navale 79, 00146 Rome, Italy

[c] IOM CNR, Laboratorio TASC, S.S. 14 Km 163.5 AREA Science Park Basovizza, Trieste 34149, Italy

[d] Department of Basic and Applied Sciences for Engineering (SBAI), Sapienza University of Rome, Via Antonio Scarpa 14, 00161 Rome, Italy

[e] Department of Anatomical, Histological, Forensic and Orthopaedic Sciences, Section of Human Anatomy, Sapienza University of Rome, Via A. Borelli 50, 00161, Rome, Italy

[f] Departamento de Ingeniería y Ciencia de los Materiales y del Transporte, Escuela Politécnica Superior, Universidad de Sevilla, Virgen de África 7, 41011 Seville Spain

*Corresponding authors
sara.cerra@uniroma1.it
ilaria.fratoddi@uniroma1.it

Graphical abstract

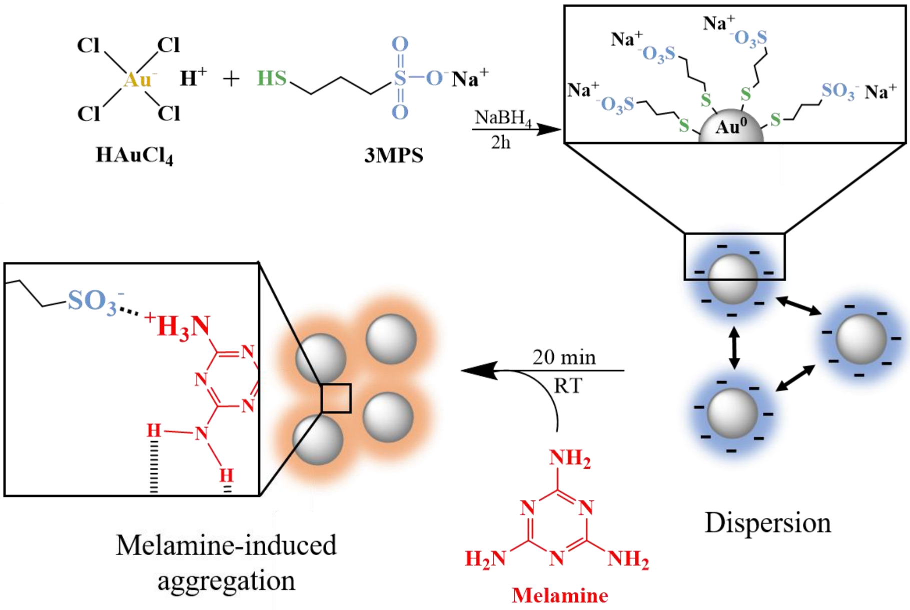
Cl
Cl
Au⁻
Cl
Cl
H⁺
+
HS
S
O
O
O⁻ Na⁺
HAuCl₄
3MPS
NaBH₄
2h
Na⁺ ⁻O₃S
Na⁺ ⁻O₃S
Na⁺ ⁻O₃S
SO₃⁻ Na⁺
S
Au⁰
SO₃⁻
⁺H₃N
N
H
H
20 min
RT
NH₂
H₂N
NH₂
Melamine
Melamine-induced aggregation
Dispersion

Abstract

In the last years, intense efforts have been made in order to obtain colloidal-based systems capable of pointing out the presence of melamine in food samples. In this work, we reported about the recognition of melamine in aqueous solutions, using gold nanoparticles stabilized with 3-mercapto-1-propanesulfonate (AuNPs-3MPS), with the aim of deepening how the recognition process works. AuNPs were synthesized using a wet chemical reduction method. The synthesized AuNPs-3MPS probe was fully characterized, before and after the recognition process, by both physicochemical (UV-vis, FT-IR, ^{1}H-NMR, DLS and ζ-potential) and morphostructural techniques (AFM, HR-TEM). The chemical and electronic structure was also investigated by SR-XPS. The sensing method is based on the melamine-induced aggregation of AuNPs; the presence of melamine was successfully detected in the range of 2.5-500 ppm. The results achieved also demonstrate that negatively charged AuNPs-3MPS are potentially useful for determining melamine contents in aqueous solution. SR-XPS measurements allowed to understand interaction mechanisms between the probe and the analyte. The presence of sulfonate groups allows a mutual interaction mediated by electrostatic bonds between nanoparticles surface thiols and positively charged amino groups of melamine molecules.

KEYWORDS: Hydrophilic gold nanoparticles; melamine; 3-mercapto-1-propanesulfonate; aggregation mechanism; electrostatic interactions

1. Introduction

1,3,5-Triazine-2,4,6-triamine – better known as Melamine – is a non-natural heterocyclic organic compound with the chemical formula $C_3H_6N_6$. Combined with formaldehyde, it produces a resin that is nowadays widely used in chemical industries to produce plastics[1], dyes[2], fertilizers[3], and fabrics[4]. However, commercial melamine has attracted critical attention since 2008, when many infants in several Chinese provinces were diagnosed with kidney stones, although this type of fraud was first documented in 2007. All of them had been fed with powdered-milk formula for infants that was later found to have been adulterated with melamine[5,6,7]. A short distance away, an estimated 300,000 babies in China were sick from the contaminated milk, and the kidney damage led to six fatalities and about 50,000 babies were hospitalized[8]. Toxic effects of melamine and its congeners have been known for decades. Ingestion of melamine leads to kidney failure and urolithiasis as symptoms of chronic poisoning[9,10]; FDA set the current limit for melamine in milk and other milk products to 1 mg/kg and 2.5 mg/kg body weight per day, respectively[11]. Toxicity of melamine is not strictly related to its structure but rather to the mechanism of hydrolysis that produces its cyanurate form[12], as shown in Scheme 1.

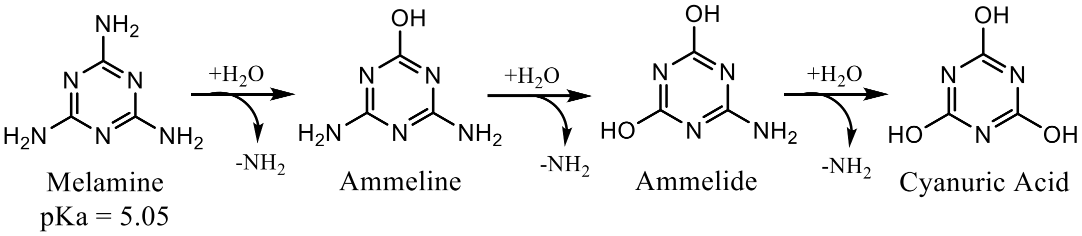

Scheme 1. Chemical structure of melamine and its derivatives obtained by hydrolysis mechanism.

In cases of food fraud, melamine is artificially added as non-protein additives to food products, e.g. milk, infant formula and pet food, in order to increase the apparent protein content[13,14]. Nitrogen content – 66% by molecular weight for melamine – has long been used as a surrogate for assessing the protein content of foods by the most common Kjeldahl assay[13]. Conventional electrochemical methods[15], hyphenated techniques such as liquid and gas chromatography-mass spectrometry (LC-MS/GC-MS)[16,17], immunosorbent assays[18], molecularly imprinted polymer (MIP)[19] and capillary electrophoresis[20] are currently used for the detection of melamine in food samples. Even though these methods are accurate and selective, lab-scale equipment is expensive, time-consuming and requires specific skills for operation[21]. For these reasons, intense efforts to devise novel efficient and simple detection systems for recognizing melamine are still under consideration[22,23,24,25,26]. The main challenge in the field of sensing is to detect low molecular weight analytes, i.e. biomolecules and contaminants, quickly, at very small concentrations and with high resolution. In this regard, great strides have been made so far in applying nanomaterials as sensors and biosensors[27,28,29,30]. Outstanding physicochemical properties are afforded by the small size of nanomaterials: high surface-to-volume ratio, variety of composition (i.e. metal, dielectric) and geometry (i.e. size, shape), unusual target binding characteristics allow to markedly enhance the response to the analytes[31]. To improve the performances, several configurations have been explored throughout the years, ranging from metallic/dielectric layers to nanostructures and thin films[26,32]. The aforementioned characteristics, together with the overall structural robustness of nanomaterials, make these materials useful in various detection configuration based on diverse recognition/transduction modes. Particularly attractive are Surface Plasmon Resonance (SPR) sensors that combine quick response with extreme sensitivity[33,34,35]. Noble metallic nanoparticles, especially gold nanoparticles (AuNPs), belong to this category, for which Localized Surface Plasmon Resonance (LSPR) is one of the most obvious properties that leads to strong absorption band in the visible/near-infrared wavelength regions. Moreover, LSPR of AuNPs can be tuned by controlling their size, shape, stabilizing agent, interparticle distance, aggregation state and dielectric constant (refractive index) of the local environment[36]. Thanks to excellent optoelectronic properties, easy fabrication process, chemical inertia, biocompatibility, and fast response various AuNPs-based colorimetric sensors have been explored over the years[37,38,39]. In this paper, we investigated the interaction mechanism that occurs between AuNPs capped with hydrophilic thiol 3-mercapto-1-propanesulfonate (3MPS) and melamine in aqueous medium. We obtained a colorimetric detection system based on electrostatic interactions between the analyte and gold nanoparticles. The effect of the molecular recognition of different standard solutions of melamine was investigated by Ultraviolet-visible (UV-vis) and Fourier-Transform Infrared spectroscopies (FT-IR). Dynamic Light Scattering (DLS) and ζ-potential analysis were able to detect the change in hydrodynamic radius ($<2R_H>$) and stability of the colloids, while morphology techniques such as Atomic Force Microscopy (AFM), High-Resolution Transmission Electron Microscopy (HR-TEM) and elemental composition analysis through Synchrotron Radiation-induced X-ray Photoelectron Spectroscopy (SR-XPS) were employed in order to confirm the tendency towards aggregation of AuNPs-3MPS after interaction with melamine.

2. Experimental section

2.1. Materials

Hydrogen tetrachloroaurate trihydrate ($HAuCl_4 \cdot 3H_2O$, 99.0%, P.M. 393.83 g/mol); sodium 3-mercapto-1-propanesulfonate ($HS(CH_2)_3SO_3Na$, 3MPS, 90.0%, P.M. 178.21 g/mol); sodium borohydride ($NaBH_4$); melamine ($C_3H_6N_6$, 1,3,5-Triazine-2,4,6-triamine, 99%, P.M. 126.12 g/mol); hydrochloric acid (HCl, ≥37%) were purchased from Sigma Aldrich and used as received. Milli-Q water (18.3 MΩ·cm) was used in all experiments. All glassware was cleaned by freshly prepared aqua regia (HCl 37%/HNO_3≥65% 3:1 by volume), rinsed thoroughly with deionized water and stored at 180°C before use.

2.2. Methods

2.2.1. Ultraviolet-Visible (UV-vis) spectroscopy

The UV–vis spectrum of aqueous colloidal gold samples was taken using a UV-vis spectrophotometer Varian Cary 100 (wavelength range of 200-800 nm) at room temperature. The quartz cells having 1 cm optical path length were used.

2.2.2. Fourier-Transform Infrared (FT-IR) spectroscopy

The FT-IR spectra of AuNPs-3MPS before and after the interaction with melamine solutions were recorded by Bruker Vertex 70 FT-IR instrument in Attenuated Total Reflection (ATR) mode at 4000-600 cm^{-1} or in transmittance mode by using KRS-5 (4 mm) windows in the range 4000-400 cm^{-1}, 16 scan rates with resolution of 4 cm^{-1}.

2.2.3. *Particle size and ζ-potential measurements*

The particle size distribution and ζ-potential measurements of the colloidal samples were carried out using Malvern Zetasizer Nano-ZS90. All the determinations were done in triplicate and data was presented in mean ± S.D. (n = 3).

2.2.4. Nuclear Magnetic Resonance (NMR) spectroscopy

^{1}H-NMR measurements were performed on a 400.13 MHz Bruker Avance III spectrometer at 9.4T. The samples were prepared in 600 μL of D_2O. The acquisition parameters for ^{1}H monodimensional experiments recorded at 295 K were: spectral width of 15 ppm, 16 scans, 6.55s repetition time to achieve full relaxation for all resonances.

2.2.5. Determination of surface morphology

The morphological characterization of AuNPs-3MPS/melamine was performed by tapping-mode Atomic Force Microscopy (AFM, Veeco Instrument, Multimode™ model equipped with a Nanoscope IIIa controller, Bruker RTESP-300 probe) on the samples prepared by drop casting onto a Si/SiO_2 substrate from their aqueous dispersion. Additionally, HR-TEM images were acquired using FEI Talos F200S FEG microscope operating at 200 keV (CITIUS central services of the University of Seville, Spain). Compositional analysis distribution was analyzed with a Super-X energy dispersive X-ray spectrometry system which includes two silicon drift detectors, couple to the microscope in the Scanning Transmission Electron Microscopy (STEM) mode, using spatial drift correction and a dwell time of 0.2 s.

Synchrotron Radiation-induced X-ray photoelectron spectroscopy (SR-XPS) measurements

SR-XPS measurements were carried out at the BACH (Beamline for Advanced DiCHroism) beamline at the ELETTRA facility in Trieste (Italy). The BACH beamline exploits the intense radiation emitted from an undulator front-end. XPS data were collected using a VG-Scienta R3000 hemispherical electron energy analyser in fixed angular mode (A21, pass energy = 50 eV), with the entrance and exit slits of the monochromator fixed at 30 μm and 20 μm, respectively. Photon energy of 360 eV was used for C1s, S2p, Au4f, spectral regions with a total binding energy resolution of 0.17 eV; for N1s and O1s spectral regions photon energy values of respectively 520 eV and 596 eV were selected, as to maximize signals intensities. The total binding energy resolution was about 0.22 eV. The energy scale was calibrated using as reference the C1s aliphatic signal at 285 eV and the $Au4f_{7/2}$ signal of AuNPs arising by metallic gold atoms, always found at 83.96 eV. Curve-fitting analysis of the C1s, S2p, N1s, O1s, Au4f spectra was performed using Gaussian curves as fitting functions. $S2p_{3/2}$, $S2p_{1/2}$ and $Au4f_{7/2}$, $Au4f_{5/2}$ doublets were fitted by using the same full width at half-maximum (FWHM) for each pair of components of the same core level, a spin–orbit splitting of 1.2 eV and 3.7 eV respectively, and branching ratios $S2p_{3/2}/S2p_{1/2} = 2/1$, $Au4f_{7/2}/Au4f_{5/2} = 4/3$. When several different species were individuated in a spectrum, the same FWHM value was used for all individual photoemission bands.

2.2.6. Gold nanoparticles AuNPs-3MPS synthesis

In this work, gold nanoparticles were synthesized as mentioned in our previous work[40]. Tetrachloroauric acid (III) trihydrate ($HAuCl_4 \cdot 3H_2O$) was used as gold ion source in the synthesis.

Sodium 3-mercapto-1-propanesulfonate ($HS(CH_2)_3SO_3Na$, 3MPS) was used as stabilizing agent in Au/S molar ratio 1/4. 0.1000g ($2.5\cdot10^{-4}$ mol) gold salt was dissolved in 10 mL of deionized water in a two-neck round-bottom flask. Gold salt was yellow at that time. After complete dissolution of the $HAuCl_4$, 10 mL aqueous solution of $1.0\cdot10^{-4}$ mol 3MPS was added. At that stage, the color of the reaction solution was observed to change suddenly to colorless, going from Au(III) to Au(I) oxidation state. The reduction of gold precursor to Au(0) was accomplished by drop wise addition of 5 mL solution of $NaBH_4$ (0.0960 g, $2.5\cdot10^{-3}$ mol) as reducing agent. Thus, the mixture was stirred for 2 hours under inert atmosphere (Ar) at +4°C. The residue, containing the AuNPs-3MPS, was washed in centrifuge at 13,400 rpm for 20 minutes with circa 30 mL of HCl 1M and 300 mL of deionized water until no sign of unreacted thiol in UV-vis absorbance spectra was observed. The obtained AuNPs-3MPS were stored at +4°C for further use (yield: 21%).

2.2.7. Preparation of melamine standard solutions

A standard stock solution of melamine with a concentration of 1 mg/mL (1000 ppm) was prepared by dissolving melamine powder in deionized water. Melamine solutions were freshly prepared by serial dilution of the ready-made stock solution with deionized water to obtain 50, 20, 10 and 5 ppm for each experimental use. The pH values of all solutions were adjusted to 4.00 ± 0.01 with HCl.

2.2.8. Interaction AuNPs-3MPS/melamine

In a typical experiment, colorimetric sensing of melamine was carried out by adding 600 μL of the synthesized AuNPs-3MPS into a fresh aliquot of 600 μL of different concentration of melamine aqueous solutions and then the mixture was shaken for 20 minutes at room temperature to obtain a stable solution.

3. Results and discussion

AuNPs stabilized with hydrophilic thiol 3-mercapto-1-propanesulfonate were used to detect different concentrations of melamine in aqueous environment, using standard solutions. The aim of this work was to assess the mechanism behind the AuNPs-3MPS/melamine interaction. As shown in Figure 1(a), UV-vis spectra exhibit a noticeable change: LSPR band displays a red shift from λ_{LSPR}=520 nm in absence of melamine up to 555 nm when AuNPs-3MPS were mixed with melamine solutions. Moreover, a broadening of plasmonic bands occurs, while the intensity of the related band gradually decreases with increasing concentration of melamine. In principle, synthetized AuNPs were stabilized against aggregation thanks to a strong negative charge of the 3MPS thiols coating the nanoparticles surface. According to DLVO theory, when nanoparticles are capped with negatively charged agents, electrostatic repulsive forces predominate over Van der Waals attractive ones, stabilizing the nanoparticles towards aggregation[41]. On the contrary, melamine is a weak base with a pK_a value of 5.05[42] and acidic conditions lead to protonation of its exocyclic amino groups ($-NH_2$). As already demonstrated in literature, recognition process shows a pH dependence with the optimum detection between pH=3.0 and pH=4.0, so we worked at this pH range for all the following experiments[43]. Understanding the principle of detection is therefore essential. AuNPs-3MPS alone exhibited a ζ-potential = -32 ± 6 mV, the presence of protonated $-NH_2$ groups linked to the aromatic ring of melamine determines an electrostatic attraction between sulfonate [-] and protonated amino group [+][44]. Consequently, ζ-potential reaches a value of -7 ± 1 mV as concentration of melamine increases (see Table 1). Moreover, due to the presence of primary amino groups in the molecular structure of melamine that act both as H-bond donors and H-bond acceptors, melamine molecules can form double hydrogen bonds (NH···N) with each other. Owing to this behavior, melamine molecules non-covalently attached on the AuNPs-3MPS surface can form intermolecular bonding with neighboring melamine molecules, determining the formation of a sort of self-assembled network[45,46]. The change of interspacing distances between AuNPs-3MPS, mediated by both electrostatic $-SO_3^-$/$-NH_3^+$ interactions and hydrogen bonds between melamine molecules, disturbs the equilibrium between electrostatic repulsive and attractive forces in favor of the latter. In these circumstances, AuNPs get unstable and quickly aggregate, which results in a red shift of the extinction maximum. Δλ values are reported in Table 2. Another evidence of the aggregation process comes from monodimensional ^{1}H-NMR experiments. As previously reported in literature,[40] ^{1}H-NMR spectra of AuNPs functionalized with 3MPS shows 3 intense signals in the range 2.00-3.00 ppm associated to $-CH_2-$ protons of the aliphatic chain; the aggregation process occurring after the mixing of colloidal gold with melamine leads to disappearance of such signals (see Figure S1, Supporting Information), mainly due to an increase in the average size of the sample that affects the correlation time of the objects.

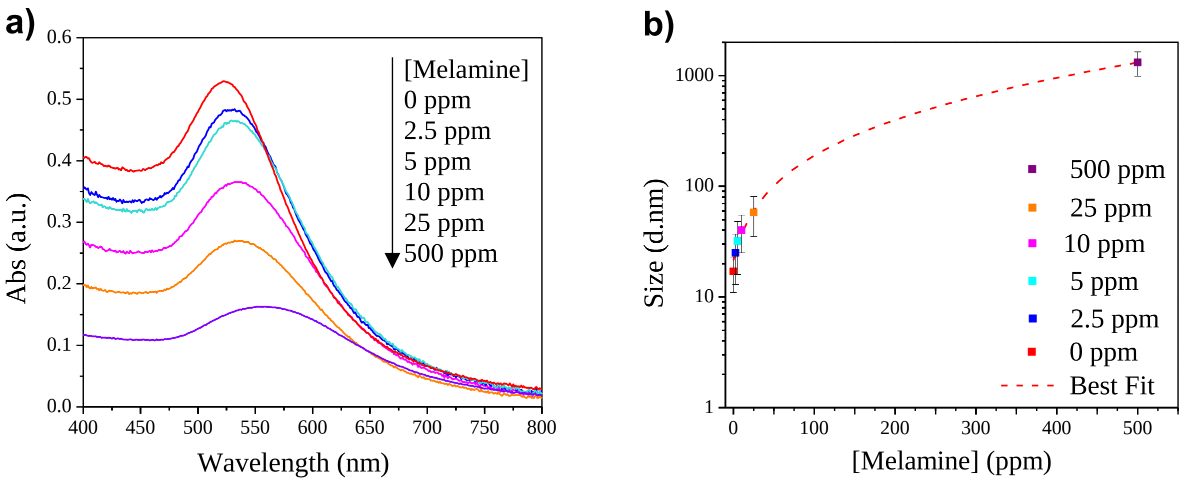

***Figure 1**. (a) Absorbance spectra of the AuNPs-3MPS obtained in the presence of different concentrations of melamine. From left to right: λ_{LSPR}=520 nm (0 ppm), λ_{LSPR}=530 nm (2.5 ppm), λ_{LSPR}=533 nm (5 ppm), λ_{LSPR}=536 nm (10 ppm), λ_{LSPR}=538 nm (25 ppm), λ_{LSPR}=560 nm (500 ppm). (b) Hydrodinamic radii of AuNPs-3MPS determined from DLS plotted vs. melamine concentration. The error bars were calculated based on the standard deviation of three measurements.*

[Melamine] (ppm)	ζ -potential (mV)
0	-32 ± 6
2.5	-25 ± 1
5	-17 ± 1
10	-22 ± 8
25	-23 ± 2
500	-7 ± 1

***Table 1**. ζ -potential values of AuNPs-3MPS in presence of different concentrations of melamine solutions.*

[Melamine] (ppm)	Δλ (nm)
2.5	+10
5	+13
10	+16
25	+18
500	+40

***Table 2**. Δλ value of AuNPs-3MPS in presence of different concentration of melamine solutions.*

The result of UV–visible spectrum was consistent with the DLS measurements showed in Figure 1(b). From the light scattering analysis, the average particle size of the AuNPs-3MPS was estimated to be 17±2 nm before the interaction with melamine samples. After hybridization with melamine, hydrodynamic diameter increased dramatically, reaching value above 1000 nm, due to aggregation process that occurs between gold nanoparticles and melamine molecules (for the size distribution of each sample see Figure S2, Supporting Information).

To better understand the interaction from a spectroscopic point of view, FT-IR measurements were performed. To do that, we investigated both pristine and protonated melamine, trying to highlight the importance of chemical environment in the recognition process. Figure 2(a) shows the comparison of FT-IR spectra of melamine before (neutral melamine) and after the exposure to HCl vapors (Mel-H$^+$). Following the blue spectra in Figure 2(a), ν(-NH$_2$) vibrations and deformation modes appear as intense bands within the region 3469-3128 cm^{-1} (3469, 3419, 3325, 3180, 3128 cm^{-1}), whereas two strong bands at 1651 cm^{-1} and 1626 cm^{-1} are assigned to δ(-NH$_2$). Bands observed at 1432 cm^{-1}, 1468 cm^{-1} and 1542 cm^{-1} are due to the ν(>C=N) and δ(-NH$_2$). Out-of-plane deformation of triazine ring is found at 810 cm^{-1}. In agreement with literature, the obtained infrared spectrum corresponds to neutral molecular form of melamine[47]. After exposure to HCl vapors a slight band shift occurs. As reported in several studies, protonation of melamine molecules can involve endocyclic N-atoms and/or exocyclic -NH$_2$ groups[47,48]; appearance of a strong band centered at ca. 1660 cm^{-1} provides evidence of triazine ring protonation resulting from exposure to HCl. Further evidence comes from the characteristic band at 813 cm^{-1}, that moves to lower frequencies (762 cm^{-1}) due to the formation of -NH$_3^+$ groups on melamine protonated molecules. Moreover, it should be noted broadening and consequent disappearance of separated bands in the 3500-3000 cm^{-1} region, with respect to neutral form, which is consistent with NH···N hydrogen bonds between protonated melamine[49]. The FTIR spectrum also provides information about the groups involved in the interaction between melamine and AuNPs-3MPS surface. Figure 2(b) shows IR spectrum of protonated melamine alone and the one of AuNPs-3MPS/melamine: the appearance of bands ν_{as}(-S=O)=1372 cm^{-1}, ν_s(-S=O)=1030 cm^{-1} and ν_s(-S-O)=670 cm^{-1} is consistent with the presence of -SO$_3^-$ groups on thiol functionalized gold nanoparticles. Changes in the δ(-NH$_2$) region (3500-3000 cm^{-1}) indicate that the interaction with thiol capped AuNPs involves a hypothetical ionic bond between protonated exocyclic -NH$_2$ groups of melamine and negatively charged SO$_3^-$ functional groups of 3MPS capping agent, meanwhile there are no differences in the 1750-1550 cm^{-1} resulting from endocyclic ring protonation.

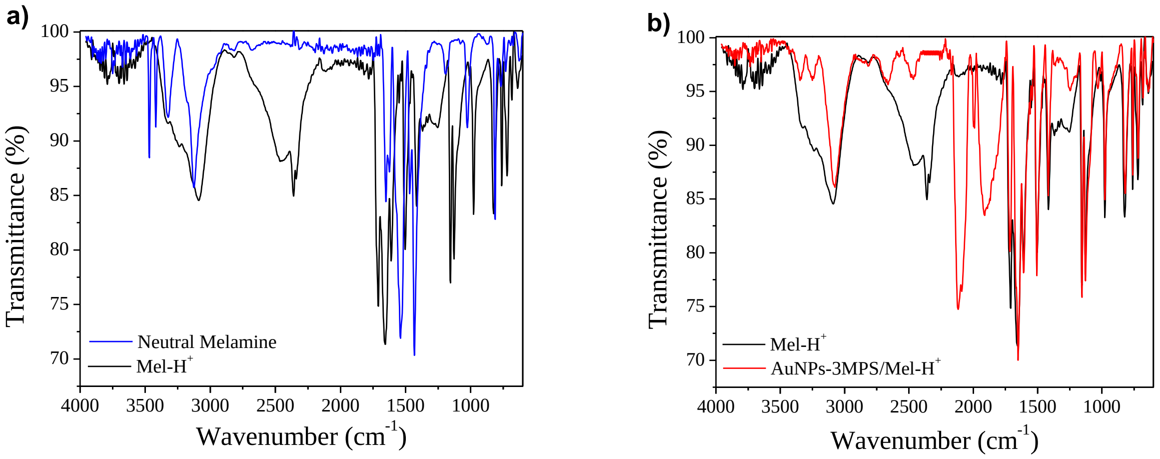

***Figure 2**. a) FT-IR spectra of melamine before (blue line) and after (black line) exposure to HCl vapors. b) Comparison of the spectra of protonated melamine (black line) and after interaction with AuNPs-3MPS sample (red line).*

3.1 Morphostructural characterizations

The size and morphology at solid state were also analyzed. 2D AFM image and the corresponding 3D projection of AuNPs-3MPS before the interaction are shown in Figure 3(a)-3(b), respectively. The as synthesized AuNPs-3MPS appear well-dispersed, showing a quite homogeneous aspect and a maximum height of ca. 5-6 nm. On the other hand, upon mixing with melamine solutions it is possible to observe the presence of aggregates. In Figure 3(c)-3(d) besides well detached objects, large agglomerations of nanoparticles are clearly visible, resulting from the melamine-induced aggregation behavior.

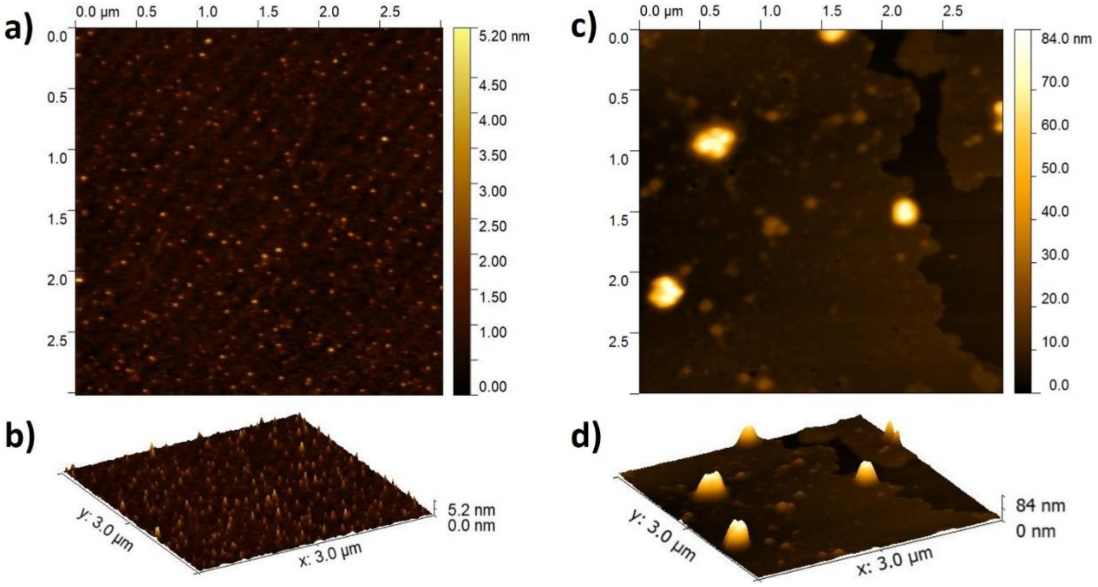

***Figure 2.** a) 2D AFM image and b) corresponding 3D projection of pristine AuNPs-3MPS. c) 2D AFM image and d) 3D projection of AuNPs-3MPS after interaction with melamine sample.*

High magnification electron microscopy observations have been acquired on the AuNPs-3MPS interacting with melamine to visualize the real impact induced by the mutual interactions of Au nanocrystals with organic species. Preliminary observation by HR-TEM image evidences the presence of dark nanostructured aggregations, as displayed in Figure 4(a). To identify the chemical composition of such dark nanostructures, EDX measurements were carried out showing the presence of gold intense peaks into the spectrum (Si, Ni and Cu peaks were from instrumental background), while the weak oxygen, nitrogen and sulfur peaks can be ascribed to the large presence of the organic species (Figure 4(b)). In particular, the small sulfur peak, shoulder of Au emission line, might be underling the presence of thiol groups covalently bound to the AuNPs-3MPS at the surface (see SR-XPS comments).

To get detailed information on the self-assembling nanostructured of gold functionalized nanoparticles interacting with melamine, the analysis of HR-TEM image by Fast Fourier Transform (FFT) and Inverse Fast Fourier Transform (IFFT) allowed to discern the mutual relationship between nanocrystals of different nature. [50] The HR-TEM image reported in Figure 4(c) clearly shows visible overlapped crystalline lattices, providing evidence of a self-assembled metal-organic network. In order to ascertain the presence of different crystalline phases from small nanocrystals embedded in the structure, the FFT analyses has been performed on selected image nanoareas of 22.76 x 22.76 nm^2. Four representative regions enclosed by short dashed blue boxes and labelled from I to IV were selected, and their corresponding FFT patterns were displayed. The I_{FFT} images reported, related to region I (Figure 4(c)), showed the nano-diffraction features of three superposition diffraction patterns. The intense inner diffraction rings have been indexed as higher-order diffraction ring (101) and its second order (202) reflection plane arose from random orientation of different crystallites (rings marked as red short dashed circles). These measured indexes are in according to the melamine crystal structure of a monoclinic system with space group *P21/n*.[51] The outer diffracted ring and two distinct diffraction spots of low intensity (orange short dashed) belong to the crystallographic lattice of gold sulfide (Au_2S). The cubic crystal system has space group *Pn3m* of (002) diffraction ring and two symmetrical reflections of (022) and (113) planes, marked by orange circles.[52] The high intensity spots (highlighted with yellow circles) represent nanocrystallites originate from the typical Au crystal of a face-centered-cubic (fcc) with a space group *Fm*3*m* and (200) reflection plane. The corresponding IFFT of the I_{FFT} image shows visible self-assembled nano-crystallites in a superimposed configuration (Figure I_{IFFT}). To discern the nanocystalline structures, the FFT contribution of the melamine or gold crystal has been subtracted before performing the inverse FFT (IFFT), for real space imaging. This procedure evidences the presence of two separate crystallites. The crystalline melamine of region I exhibits overlapped fringes with the lattice spacing of d_{220} = 0.59 and d_{220} =

0.30 nm (red arrowed, Figure I_{mel}), while the super position of pure Au and functionalized Au crystallites are well visible in the IFFT of same region (Figure I_{Au}). Herein, two adjacent crystallites of pure Au of d_{200} = 0.20 nm (yellow short dashed lines and yellow arrowed) show lattice fringe partially overlapped by the lattice fringe of the Au_2S crystallites (d_{002} = 0.1.75 and d_{113} = 0.154 nm, orange arrowed) and separated Au_2S lattice fringes (d_{113} = 0.25 nm, orange arrowed) can be observed. It should be added that the observed different intensity of the lattice fringes can be related to different height of the focal plane imaging intersecting the atomic layers at different heights along the axis normal to the image plane. In order to better show the alone crystalline contributions of the melamine, the region II of Figure 4(c) was selected. The II_{FFT} nanoregion of the alone melamine has been identified the preferential orientations of the crystallographic (101) and (202) planes. The corresponding I_{IFFT} images evidences the mutual crystallographic interaction among the planes. By subtracting the crystallographic (202) diffraction contribution, broad lattice fringes of (101) plane with lattice spacing of 0.59 nm are well shown (Figure II_{mel}); whereas I_{IFFT} image, representing the second order reflection plane (202) of 0.30 nm lattice spacing, was characterized by long and narrow lattice fringes that may be attributed to the intrinsic property of the small melamine molecules in stacking configuration. The selected region III of peculiar structural property has been proposed to show on how crystalline melamine self-assembled with amount of Au functionalized crystallites at small nanometric dimension. The analysis of the nano-diffraction pattern of III_{FFT} image exhibits the presence of several superimposed patters. Figure III_{IFFT} confirmed the mutual interaction of crystalline melamine lattices surrounded by Au_2S and Au pure nanocrystallites by analysing the corresponding separate contributions. Figure III_{mel} shows the crystalline melamine lattices well overlapped (d_{101220} = 0.59 and d_{20220} = 0.30 nm) as well as the Au_2S and Au pure crystallites, superimposing melamine lattices in red short dashed line (Figure III_{Au}). It was also interesting to show the structural contribution of the Au_2S nanocrystallites surrounding the melamine molecules in the selected region IV. By comparing Figure IV_{mel} and Figure IV_{Au}, high amount of Au_2S crystallites formed a layer of connected nanocrystallites with melamine. The lattice crystalline layer of functionalized Au exhibited different orientation lattice probably due to the growth of gold crystal seed during the interaction with melamine broad lattice fringes (Figure IV_{Au}).[53] This result was further supported by the finding of the techniques above discussed. To the best of our knowledge, a full understanding of the growth mechanism of Au nanoparticles interacting with melamine is still a challenging task, although HR-TEM imaging analysis have shown that the gold functionalized nanoparticles easily entrap the melamine structure, starting from their initial mutual interaction at nanoscopic scale.

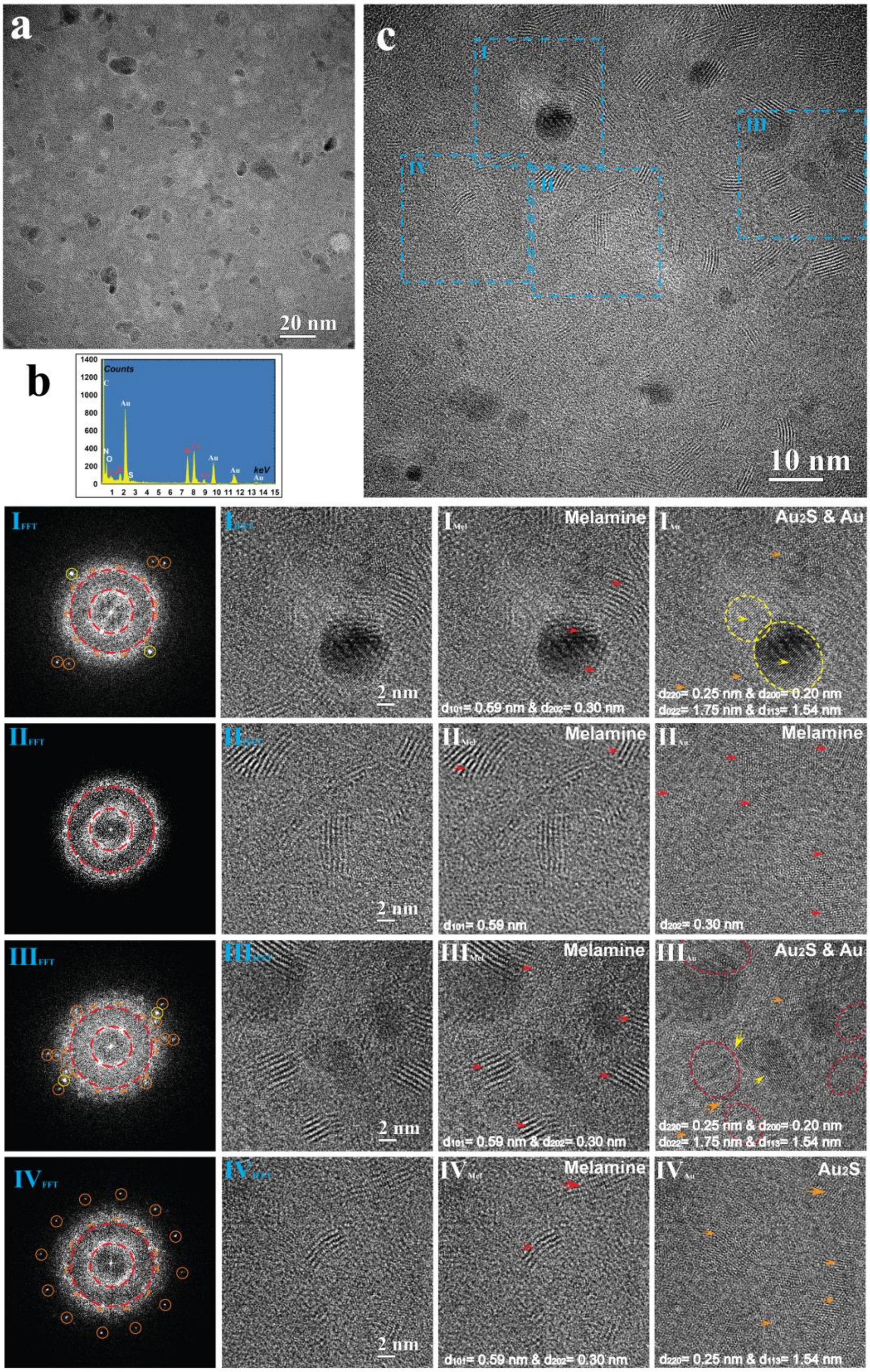

Figure 4. *Evidence of Au-melamine nanocrystals from High resolution TEM. (a) HR-TEM image of Au-melamine system.* ***(b)*** *EDX spectral image probed on Fig. 3a.* ***(c)*** *High resolution TEM image of Au-melamine system. Inset: four representative regions enclosed by short dashed blue boxes and labelled by roman numbers from I to IV were selected. The corresponding FFT patterns with the sequential IFFT images and their subtracted contributions are displayed.*

To further investigate the effectiveness of melamine coordination to AuNPs as well as to attempt to individuate the functional groups involved in the AuNPs/melamine interaction SR-XPS measurements were carried out at C1s, O1s, S2p, Au4f and N1s core levels of both AuNPs-3MPS/melamine and the pristine AuNPs-3MPS. SR-XPS data analysis results (Binding Energy – BE -, Full Width Half Maxima – FWHM -, Atomic percentages and proposed assignments for all measured signals components) are collected in Table S1 in the Supporting Information.

Au4f and S2p core level spectra are usually considered as the most indicative for the assessment of ligands/noble metal interaction; in excellent agreement with the results reported for analogous AuNPs-3MPS systems,[54] gold spectra of both samples show a main peak at about 83.9 eV due to metallic gold atoms in NPs bulk, and a small shoulder a higher BE values (about 84.8 eV BE, 10% of whole Au4f signal intensity) assigned to positively charged gold atoms at the NP surface, chemically interacting with the thiol functional groups of 3MPS (see Table S1, Supporting Information). S2p spectra of AuNPs-3MPS/melamine and AuNPs-3MPS are reported in Figure 5(a) and Figure 5(b) respectively; both spectra are composites, and four spin-orbit pairs can be individuated by applying a peak-fitting procedure. Starting from the peaks at lower Binding Energy, the four S2p components can be attributed to: RS-Au (thiols covalently bonded to gold atoms at the NP surface) ($S2p_{3/2}$ BE = 161.5 eV), physisorbed RS-H thiol groups ($S2p_{3/2}$ BE = 163.5 eV), and sulfonate functional groups. Although S2p spectra are analogous for the two samples in the thiol-related part (R-S-Au and R-S-H signals), a difference can be observed in the signals components attributed to sulfonates; as shown in Figure 5(b), the $S2p_{3/2}$ peaks related to sulfonate moieties are centered at 167.01 eV ($R\text{-}SO_3^-$) and 168.6 eV ($R\text{-}SO_3Na$) for the pristine AuNPs-3MPS, as already observed for analogous systems[55]; on the other hand, in AuNPs-3MPS/melamine (Figure 5(a)) the $S2p_{3/2}$ peak associated with $R\text{-}SO_3^-$ is shifted at lower BE (165.41 eV). The peak at higher BE ($R\text{-}SO_3Na$) is stable at about 168.6 eV. The chemical shift of the sulfonate-related component suggests an electron-acceptor behavior for the sulfonate moiety, that can be hypothesized to contribute to the interaction of AuNPs-3MPS with melamine.

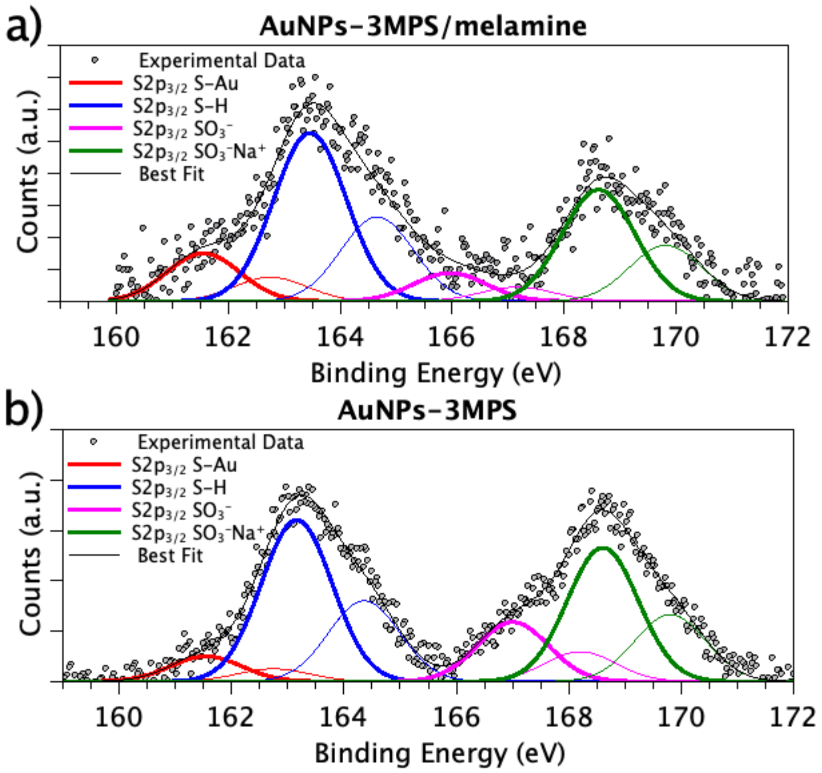

Figure 5. *S2p core-level spectra of a) AuNPs-3MPS/melamine, b) AuNPs-3MPS. In magenta, the spectral components associated with sulfonate functional groups.*

The analysis of N1s core level signal allows to gather useful information about the melamine/AuNPs-3MPS interaction. N1s spectrum of AuNPs-3MPS/melamine (see Figure 6) is asymmetric, allowing to individuate two main contributions at 398.80 eV and 400.59 eV BE. The peak at lower BE is attributed to pyridine-like N of the melamine rings, as well as amine pending groups of the ring (NIST X-ray Photoelectron Spectroscopy Database, Version 4.1, National Institute of Standards and Technology, Gaithersburg, 2012; http://srdata.nist.gov/xps/); the lower intensity signal at 400.59 eV BE is usually attributed to positively charged amines ($R-NH_3^+$). [55] This last signal allows to hypothesize that some amine groups are positively charged, and they interact with the negatively charged sulfonate groups of 3MPS moieties.

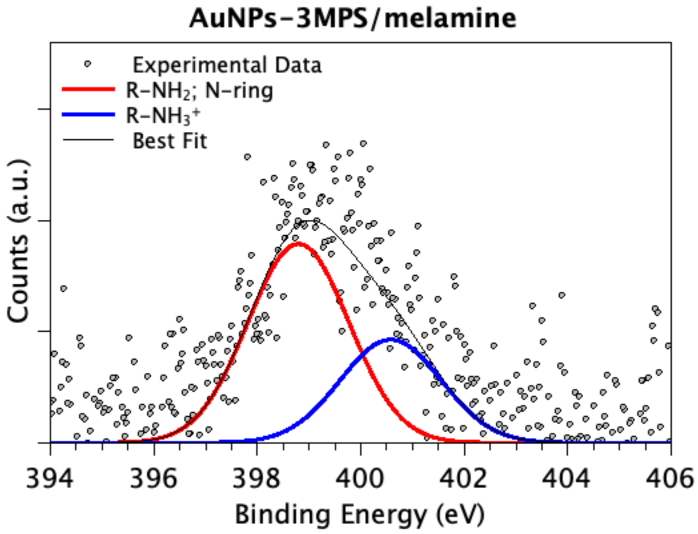

Figure 6. *SR-XPS N1s core-level spectrum of AuNPs-3MPS/melamine. The blue component is indicative for protonated amine groups, that are hypothesized to interact with negatively charged sulfonate moieties of AuNPs-3MPS.*

4. *Conclusions*

Based on recent literature, thiol capped gold nanoparticles are gaining growing interest for sensing of melamine in food samples. In this framework, a deep understanding of the mechanisms involved in the recognition process was needed. Focusing on gold nanoparticles stabilized with negatively charged 3-mercapto-1-propanesulfonate, we demonstrated here the capability of this colloidal system to point out the presence of melamine in aqueous solution in the 2.5-500 ppm range. AuNPs-3MPS before and after interaction with melamine were characterized on LSPR phenomena, mean particle size, surface potential, morphology and structure. Specifically, UV-Vis measurements highlight the broadening and red shift of LSPR band of AuNPs-3MPS, according to an increase in the mean particles size from 17±2 nm up to 1000 nm and progressive decrease in surface potential, as demonstrated by DLS and ζ-potential measurements, respectively. The AFM and HR-TEM analyses provide further and deeper details in morphostructural features. The recognition process involves formation of aggregates in which AuNPs-3MPS easily entrap the melamine structure, starting from their initial mutual interaction at nanoscopic scale. Moreover, FT-IR measurements also provide information about the groups involved in the interaction between gold nanoparticles surface and melamine molecules. It was found that melamine owns $-NH_3^+$ groups able to interact with $-SO_3^-$ groups of thiols functionalizing nanoparticles, guiding the aggregation process, as confirmed by SR-XPS data. These results will be helpful to improve the knowledge about gold colloids-based sensors, since the surface functionalization and charge of AuNPs can be tailored to obtain specific interaction with melamine minimizing the interference effects in real matrices.

Acknowledgments

The authors want to thank the Universidad de Sevilla (Spain) for the use of TEM experimental facilitates at CITIUS, Microscopy (funding by VI PPIT-2019-I.5 Isabel Montealegre Meléndez).

IF gratefully acknowledge Ateneo Sapienza grants Sapienza 2019 RM11916B75D8FAF5 and 2017 RM11715C792D1AF3. SC acknowledges Sapienza grant Avvio alla Ricerca 2020 AR120172A75F8B3A. SN acknowledge financial support from MUR (Eurofel project, FOE progetti internazionali).

SUPPORTING INFORMATION

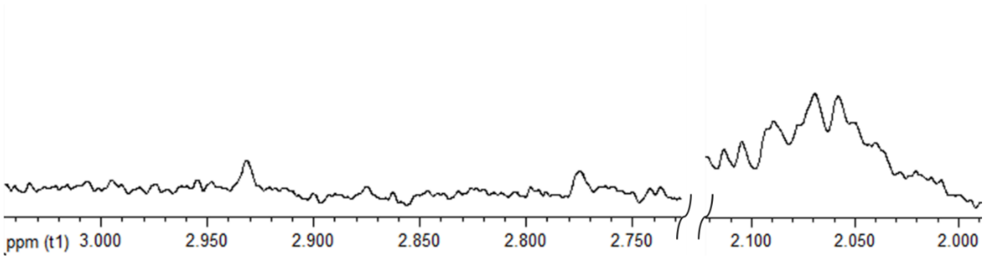

Figure S1. *^{1}H resonances of AuNPs-3MPS/melamine.*

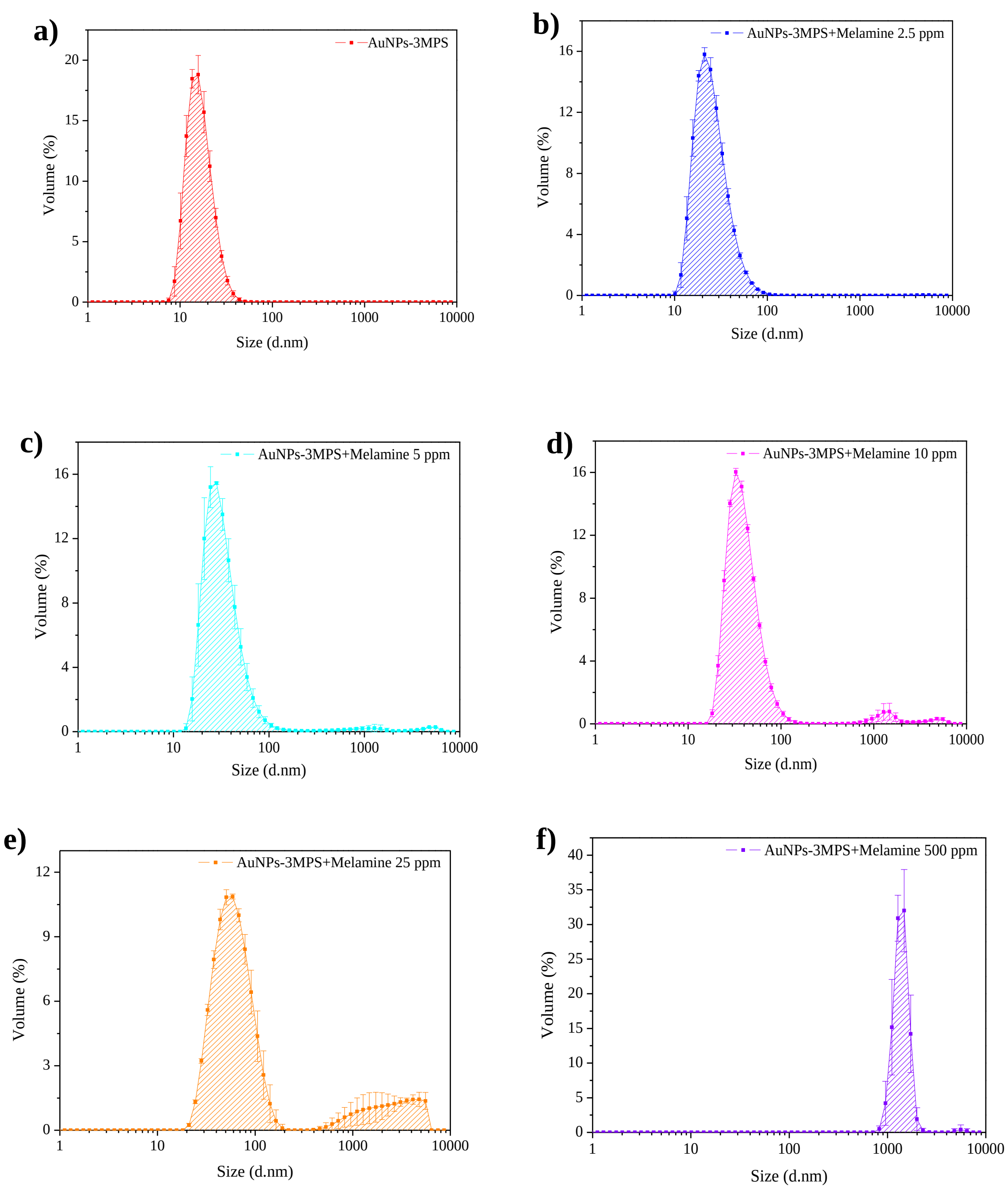

Figure S2. *DLS size distributions of the samples.*

***Table S1**. Binding Energy, Full Width Half Maxima, Atomic percentages and proposed assignments for all measured signals components of AuNPs-3MPS/melamine and AuNPs-3MPS*

SAMPLE	SIGNAL	BE (eV)	FWHM (eV)	Atomic %*	Assignment
AuNPs-3MPS/melamine	C1s	285.00	1.26		C-C
		286.29	1.26		C-N, C-S
		287.43	1.26		C=O
		288.96	1.26		COOH
	N1s	398.80	2.29	65.8	R-NH$_2$, N-ring
		400.59	2.29	34.2	R-NH$_3^+$
	S2p$_{3/2}$	161.55	1.50	13.4	RS-Au
		163.47	1.50	47.3	RS-H
		165.41	1.50	7.9	RSO$_3^-$
		168.60	1.50	31.4	RSO$_3$Na
	Au4f$_{7/2}$	83.98	0.84	87.7	
		84.50	0.84	12.3	
AuNPs-3MPS	C1s	285.00	1.10		C-C
		286.02	1.10		C-N, C-S
		287.13	1.10		C=O
		288.48	1.10		COOH
	S2p$_{3/2}$	161.53	1.44	6.6	RS-Au
		163.17	1.44	42.5	RS-H
		167.01	1.44	15.6	RSO$_3^-$
		168.60	1.44	35.2	RSO$_3$Na
	Au4f$_{7/2}$	83.96	0.81	90.0	
		84.83	0.81	10.0	

* the statistical incertitude in semiquantitative evaluation by XPS is estimated as 5% of the calculated value[56]

References

---

[1] Chen, X.; Zhang, X.; Wang, W.; Wang, Y.; Jiao, C. Fire-safe agent integrated with oyster shell and melamine polyphosphate for thermoplastic polyurethane. *Polym. Adv. Technol.* **2019**, *30*, 1576-1588. https://doi.org/10.1002/pat.4588.

[2] Chen, J.; Jiang, M.; Han, J.; Liu, K.; Liu, M.; Wu, Q. Syntheses of magnetic GO@melamine formaldehyde resin for dyes adsorption. *Mater. Res. Express* **2019**, *6*, 086103. https://doi.org/10.1088/2053-1591/ab1ba6.

[3] Giroto, A.S.; Garcia, R.H.S.; Colnago, L.A.; Klamczynski, A.; Glenn, G.M.; Ribeiro, C. Role of urea and melamine as synergic co-plasticizers for starch composites for fertilizer application. *Int. J. Biol. Macromol.* **2020**, *144*, 143-150. https://doi.org/10.1016/j.ijbiomac.2019.12.094.

[4] Saraç, E.G.; Öner, E.; Kahraman, M.V. Microencapsulated organic coconut oil as a natural phase change material for thermo-regulating cellulosic fabrics. *Cellulose* **2019**, *26*, 8939-8950. https://doi.org/10.1007/s10570-019-02701-9.

[5] Dobson, R.L.M.; Motlagh, S.; Quijano, M.; Cambron, R.T.; Baker, T.R.; Pullen, A.M.; Regg, B.T.; Bigalow-Kern, A.S.; Vennard, T.; Fix, A.; Reimschuessel, R.; Overmann, G.; Shan, Y.; Daston, G.P. Identification and characterization of toxicity of contaminants in pet food leading to an outbreak of renal toxicity in cats and dogs. *Toxicol. Sci.* **2008**, *106*, 251-262. https://doi.org/10.1093/toxsci/kfn160.

[6] Chen, J.-S. A worldwide food safety concern in 2008-melamine-contaminated infant formula in China caused urinary tract stones in 290 000 children in China. *Chin. Med. J.* **2009**, *122*, 243-244. https://doi.org/10.3760/cma.j.issn.0366-6999.2009.03.001.

[7] Gossner, C.M.E.; Schlundt, J.; Ben Embarek, P.; Hird, S.; Lo-Fo-Wong, D.; Beltran, J.J.O.; Teoh, K.N.; Tritscher, A. The melamine incident: implications for international food and feed safety. *Environ. Health Perspect.* **2009**, *117*, 1803-1808. https://doi.org/10.1289/ehp.0900949.

[8] Li, Q.; Song, P.; Wen, J. Melamine and food safety: a 10-year review. *Curr. Opin. Food Sci.* **2019**, *30*, 1-6. https://doi.org/10.1016/j.cofs.2019.05.008.

[9] Chang, H.; Shi, X.; Shen, S.; Wang, W.; Yue, Z. Characterization of melamine-associated urinary stones in children with consumption of melamine-contaminated infant formula. *Clin. Chem. Acta* **2012**, *413*, 985-991. https://doi.org/10.1016/j.cca.2012.02.025.

[10] Liu, C.-C.; Wu, C.-F.; Chen, B.-H.; Huang, S.-P.; Goggins, W.; Lee, H.-H.; Chou, Y.-H.; Wu, W.-J.; Huang, C.-H.; Shiea, J.; Lee, C.-H.; Wu, K.-Y.; Wu, M.-T. Low exposure to melamine increases the risk of urolithiasis in adults. *Kidney Int.* **2011**, *80*, 746–752. https://doi.org/10.1038/ki.2011.154.

---

[11] Li, Y.; Xu, J.; Sun, C. Chemical Sensors and Biosensors for the Detection of Melamine. *RSC Adv.* **2015**, *5*, 1125-1147. https://doi.org/10.1039/C4RA13080D.

[12] Bozzi, A.; Dhananjeyan, M.; Guasaquillo, I.; Parra, S.; Pulgarin, C.; Weins, C.; Kiwi, J. Evolution of toxicity during melamine photocatalysis with TiO_2 suspensions. *J. Photochem. Photobiol. A* **2004**, *162*, 179-185. https://doi.org/10.1016/S1010-6030(03)00352-6.

[13] Xiu, C.; Klein, K.K. Melamine in milk products in China: Examining the factors that led to deliberate use of the contaminant. *Food Policy* **2010**, *35*, 463-470. https://doi.org/10.1016/j.foodpol.2010.05.001.

[14] Hau, A.K.-C.; Kwan, T.H.; Li, P.K.-M. Melamine toxicity and the kidney. *J. Am. Soc. Nephrol.* **2009**, *20*, 245-250. https://doi.org/10.1016/j.foodpol.2010.05.001.

[15] Tsai, T.-H.; Thiagarajan, S.; Chen, S.-M. Detection of melamine in milk powder and human urine. *J. Agric. Food Chem.* **2010**, *58*, 4537-4544. https://doi.org/10.1021/jf904554s.

[16] El-Sheikh, A.H.; Al-Degs, Y.S.; Abu-Wardeh, A.H.; Al-Ghouti, M.A. Quantification of melamine in milk and dairy products by liquid chromatography after a simple sample clean-up procedure. *J. Food Process. Preserv.* **2016**, *41*, e12867. https://doi.org/10.1111/jfpp.12867.

[17] Miao, H.; Fan, S.; Wu, Y.-N.; Zhang, L.; Zhou, P.-P.; Chen, H.-J.; Zhao, Y.-F.; Li, J.-G. Simultaneous determination of melamine, ammelide, ammeline, and cyanuric acid in milk and milk products by gas chromatography-tandem mass spectrometry. *Biomed. Environ. Sci.* **2009**, *22*, 87-94. https://doi.org/10.1016/S0895-3988(09)60027-1.

[18] Zhou, Y.; Li, C.-Y.; Li, Y.-S.; Ren, H.-L.; Lu, S.-Y.; Tian, X.-L.; Hao, Y.-M.; Zhang, Y.-Y.; Shen, Q.-F.; Liu, Z.-S.; Meng, X.-M.; Zhang, J.-H. Monoclonal antibody based inhibition ELISA as a new tool for the analysis of melamine in milk and pet food samples. *Food Chem.* **2012**, *135*, 2681-2686. https://doi.org/10.1016/j.foodchem.2012.07.053.

[19] Bengamra, M.; Grayaa-Jaoued, N.; Khlifi-Riani, A.; Chehimi, M.M.; Kalfat, R. Highly selective molecularly imprinted sol-gel membrane grafted to gold for the detection of melamine. *Silicon* **2019**, *11*, 2267-2274. https://doi.org/10.1007/s12633-017-9674-2.

[20] Wen, Y.; Liu, H.; Han, P.; Gao, Y.; Luan, F.; Li, X. Determination of melamine in milk powder, milk and fish feed by capillary electrophoresis: a good alternative to HPLC. *J. Sci. Food Agric.* **2010**, *90*, 2178-2182. https://doi.org/10.1002/jsfa.4066.

[21] Liu, Y.; Todd, E.E.D.; Zhang, Q.; Shi, J.-R.; Liu, X.-J. Recent developments in the detection of melamine. *J. Zhejiang Univ. Sci. B.* **2012**, *13*, 525–532. https://doi.org/10.1631/jzus.B1100389.

[22] Lim, J.; Kim, G.; Mo, C.; Kim, M.S.; Chao, K.; Qin, J.; Fu, X.; Baek, I.; Cho, B.-K. Detection of melamine in milk powders using near-infrared hyperspectral imaging combined with regression

---

coefficient of partial least square regression model. *Talanta* **2016**, *151*, 183-191. https://doi.org/10.1016/j.talanta.2016.01.035.

[23] Sheng, Y.; You, Y.; Cao, Z.; Liu, L.; Wu, H.-C. Rapid and selective DNA-based detection of melamine using α-hemolysin nanopores. *Analyst.* **2018**, *143*, 2411-2415. https://doi.org/10.1039/C8AN00580J.

[24] Su, R.; Zheng, H.; Dong, S.; Sun, R.; Qiao, S.; Sun, H.; Ma, X.; Zhang, T.; Sun, C. Facile detection of melamine by a FAM–aptamer–G-quadruplex construct. *Anal. Bioanal. Chem.* **2019**, *411*, 2521-2530. https://doi.org/10.1007/s00216-019-01688-3.

[25] Zhuang, Q.; Li, L.; Ding, Y.; Zeng, H.; Wu, Y. Highly luminescent nitrogen-doped carbon dots as “turn-on” fluorescence probe for selective detection of melamine. *ChemistrySelect* **2019**, *4*, 84-89. https://doi.org/10.1002/slct.201803471.

[26] Xu, D.; Kang, W.; Zhang, S.; Yang, W.; Lei, Y.; Chen, J. Quantitative determination of melamine in milk by surface-enhanced Raman scattering technique based on high surface roughness silver nanosheets assembled by nanowires. *Microchem. J.* **2019**, *148*, 190-196. https://doi.org/10.1016/j.microc.2019.04.077.

[27] La Spada, L.; Vegni, L. Electromagnetic nanoparticles for sensing and medical diagnostic applications. *Materials* **2018**, 11, 603. https://doi.org/10.3390/ma11040603.

[28] Bearzotti, A.; Papa, P.; Macagnano, A.; Zampetti, E.; Venditti, I.; Fioravanti, R.; Fontana, L.; Matassa, R.; Familiari, G.; Fratoddi, I. Environmental Hg vapors adsorption and detection by using functionalized gold nanoparticles network. *J. Environ. Chem. Eng.* **2018**, *6*, 4706-4713. https://doi.org/10.1016/j.jece.2018.07.013.

[29] Mochi, F.; Burratti, L.; Fratoddi, I.; Venditti, I.; Battocchio, C.; Carlini, L.; Iucci, G.; Casalboni, M.; De Matteis, F.; Casciardi, S.; Nappini, S.; Pis, I.; Prosposito, P. Plasmonic sensor based on interaction between silver nanoparticles and Ni^{2+} or Co^{2+} in water. *Nanomaterials* **2018**, *8*, 488. https://doi.org/10.3390/nano8070488.

[30] Zhao, N.; Li, H.; Tian, C.; Xie, Y.; Feng, Z.; Wang, Z.; Yan, X.; Wang, W.; Yu, H. Bioscaffold arrays decorated with Ag nanoparticles as a SERS substrate for direct detection of melamine in infant formula. *RSC Adv*. **2019**, *9*, 21771-21776. https://doi.org/10.1039/C9RA01862J.

[31] Aragay, G.; Pino, F.; Merkocį, A. Nanomaterials for sensing and destroying pesticides. *Chem. Rev.* **2012**, *112*, 5317−5338. https://doi.org/10.1021/cr300020c.

[32] Fratoddi, I.; Matassa, R.; Fontana, L.; Venditti, I.; Familiari, G.; Battocchio, C.; Magnano, E.; Nappini, S.; Leahu, G.; Belardini, R.; Li Voti, R.; Sibilia, C. Electronic properties of a functionalized noble metal nanoparticles covalent network. *J. Phys. Chem. C* **2017**, *121*, 18110-18119. https://doi.org/10.1021/acs.jpcc.7b07176.

---

[33] Wu, H.; Li, H.; Chua, F.Z.H.; Li., S.F.Y. Rapid detection of melamine based on immunoassay using portable surface plasmon resonance biosensor. *Sens. Actuators B Chem.* **2013**, *178*, 541-546. https://doi.org/10.1016/j.snb.2012.12.089.

[34] Varun, S.; Kiruba Daniel, S.C.G.; Gorthi, S. S. Rapid sensing of melamine in milk by interference green synthesis of silver nanoparticles. *Mater. Sci. Eng. C.* **2017**, *74*, 253-258. https://doi.org/10.1016/j.msec.2016.12.011.

[35] Zhou, J.; Qi, Q.; Wang, C.; Qian, Y.; Liu, G.; Wang, Y.; Fu, L. Surface plasmon resonance (SPR) biosensors for food allergen detection in food matrices. *Biosens. Bioelectron.* **2019**, *142*, 111449. https://doi.org/10.1016/j.bios.2019.111449.

[36] Kang, H.; Buchman, J.T.; Rodriguez, R.S.; Ring, H.L.; He, J.; Bantz, K.C.; Haynes, C.L. Stabilization of silver and gold nanoparticles: preservation and improvement of plasmonic functionalities. *Chem. Rev.* **2019**, *119*, 664-699. https://doi.org/10.1021/acs.chemrev.8b00341.

[37] Li, C.M.; Zhen, S.J.; Wang, J.; Li, Y.F.; Huang, C.Z. A gold nanoparticles-based colorimetric assay for alkaline phosphatase detection with tunable dynamic range. *Biosens. Bioelectron.* **2013**, *43*, 366-371. https://doi.org/10.1016/j.bios.2012.12.015.

[38] Liang, X.; Wei, H.; Cui, Z.; Deng, J.; Zhang, Z.; Youab, X.; Zhang, X.-E. Colorimetric detection of melamine in complex matrices based on cysteamine-modified gold nanoparticles. *Analyst.* **2011**, *136*, 179. https://doi.org/10.1039/C0AN00432D.

[39] Paul, I.E.; Rajeshwari, A.; Prathna, T.C.; Raichur, A.M.; Chandrasekarana, N.; Mukherjee, A. Colorimetric detection of melamine based on the size effect of AuNPs. *Anal. Methods* **2015**, *7*, 1453-1462. https://doi.org/10.1039/C4AY02622E.

[40] Venditti, I.; Fontana, L.; Fratoddi, I.; Battocchio, C.; Cametti, C.; Sennato, S.; Mura, F.; Sciubba, F.; Delfini, M.; Russo, M.V. Direct interaction of hydrophilic gold nanoparticles with dexamethasone drug: Loading and release study. *J. Colloid Interface Sci.* **2014**, *418*, 52-60. https://doi.org/10.1016/j.jcis.2013.11.063.

[41] Ahmad, N.S.; Radiman, S.; Yaacob, W.Z.W. Aggregation and stability of iron oxide and alumina nanoparticles: influences of pH and humic acid concentration. *Sains Malays.* **2019**, *48*, 435-442. https://doi.org/10.17576/jsm-2019-4802-22.

[42] Ping, H.; Zhang, M.; Li, H.; Li, S.; Chen, Q.; Sun, C.; Zhang, T. Visual detection of melamine in raw milk by label-free silver nanoparticles. *Food Control* **2012**, *23*, 191-197. https://doi.org/10.1016/j.foodcont.2011.07.009.

[43] Liang, X.; Wei, H.; Cui, Z.; Deng, J.; Zhang, Z.; You, X.; Zhang, X.-E. Colorimetric detection of melamine in complex matrices based on cysteamine-modified gold nanoparticles. *Analyst.* **2011**, *136*, 179-183. https://doi.org/10.1039/C0AN00432D.

---

[44] Wu, L.; Chen, K.; Lu, Z.; Li, T.; Shao, K.; Shao, F.; Han, H. Hydrogen-bonding recognition-induced aggregation of gold nanoparticles for the determination of the migration of melamine monomers using dynamic light scattering. *Anal. Chim. Acta* **2014**, *845*, 92-97. https://doi.org/10.1016/j.aca.2014.07.036.

[45] Silly, F.; Shaw, A.Q.; Castell, M.R.; Briggs, G.A.D.; Mura, M.; Martsinovich, N.; Kantorovich, L. Melamine structures on the Au(111) surface. *J. Phys. Chem. C* **2008,** *112*, 11476-11480. https://doi.org/10.1021/jp8033769.

[46] Uemura, S.; Aono, M. Komatsu, T.; Kunitake, M. Two-dimensional self-assembled structures of melamine and melem at the aqueous solution-Au(111) interface. *Langmuir* **2011**, *27,* 1336-1340. https://doi.org/10.1021/la103948n.

[47] Mircescu, N.E.; Oltean, M.; Chis, V.; Leopold, N. FTIR, FT-Raman, SERS and DFT study on melamine. *Vib. Spectrosc.* **2012**, *62*, 165-171. https://doi.org/10.1016/j.vibspec.2012.04.008.

[48] Drozd, M.; Marchewka, M.K. The structure, vibrational spectra and nonlinear optical properties of neutral melamine and singly, doubly and triply protonated melaminium cations—theoretical studies. *J. Mol. Struct.* **2005**, *716*, 175-192. https://doi.org/10.1016/j.theochem.2004.11.020.

[49] Wang, S.; Huang, F.; Zhou, L.; Wei, J.; Xin, Y.; Jin, P.; Cai, Z.; Yin, Z.; Pang, Q.; Zhang, J.Z. Enhanced photoluminescence and stability of $CH_3NH_3PbBr_3$ perovskite nanocrystals with protonated melamine. *Chem. Nano Mat.* **2018**, *4*, 1-9. https://doi.org/10.1002/cnma.201800006.

[50] Matassa, R.; Orlanducci, S.; Reina, G.; Cassani, M.C.; Passeri, S.; Terranova, M.L. Structural and morphological peculiarities of hybrid Au/nanodiamond engineered nanostructures. *Sci. Rep.* **2016**, *6,* 31163. https://doi.org/10.1038/srep31163.

[51] Li, P.; Arman, H. D.; Wang, H.; Weng, L.; Alfooty, K.; Angawi, R. F.; Chen, B. Solvent dependent structures of melamine: Porous or nonporous? *Cryst. Growth Des.* **2015**, *15*, 1871-1875. https://doi.org/10.1021/acs.cgd.5b00039.

[52] Ishikawa, K.; Isonaga, T.; Wakita, S.; Suzuki, Y. Structure and electrical properties of Au_2S. *Solid State Ion.* **1995**, *79*, 60-66. https://doi.org/10.1016/0167-2738(95)00030-A.

[53] Matassa, R.; Familiari, G.; Battaglione, E.; Sibilia, C.; Leahu, G.; Belardini, A.; Venditti, I.; Fontana, L.; Fratoddi, I. Electron microscopy reveals layered architecture of individual gold nanoparticles self-anchored by fluorescence monomers. *Nanoscale* **2016**, *8,* 18161-18169. https://doi.org/10.1039/C6NR06260A.

[54] Carlini, L.; Fasolato, C.; Postorino, P.; Fratoddi, I.; Venditti, I.; Testa, G.; Battocchio, C. Comparison between silver and gold nanoparticles stabilized with negatively charged hydrophilic

---

thiols: SR-XPS and SERS as probes for structural differences and similarities. *Colloids Surf. A Physicochem. Eng. Asp.* **2017**, *532*, 183-188. https://doi.org/10.1016/j.colsurfa.2017.05.045.

[55] Secchi, V.; Franchi, S.; Ciccarelli, D.; Dettin, M.; Zamuner, A.; Serio, A.; Iucci, G.; Battocchio, C. Biofunctionalization of TiO_2 surfaces with self-assembling layers of oligopeptides covalently grafted to chitosan. *ACS Biomater. Sci. Eng.* **2019**, *5*, 2190-2199. https://doi.org/10.1021/acsbiomaterials.9b00430.

[56] Swift, P.; Shuttleworth, D.; Seah, M. P. Practical surface analysis by auger and x-ray photoelectron spectroscopy, Briggs, D.; Seah, M. P. (Eds).; J. Wiley & Sons, Chichester, 1983, chapter 4.